[21] Hyperspectral and multispectral RESURS-P data fusion to increase their informational content

Anshakov G.P. , Raschupkin A.V. , Zhuravel Y.N.
Samara Scientific Center of the Russian Academy of Sciences
JSC "RSC Progress", Samara

Abstract

RESURS-P spacecraft enables to observe underlying surface using both multi– and hyperspectral equipment at the same time. The multispectral images received have high spatial but low spectral resolution. Hyperspectral images, on the contrary, have high spectral but low spatial resolution. This article is devoted to the hyper– and multispectral data fusion method of information properties improvement.

Keywords: *remote sensing, hyperspectral imaging, multispectral imaging, spatial resolution, spectral resolution.*

Citation: *Anshakov G.P. Hyperspectral and multispectral Resurs-P data fusion to increase their informational content / Anshakov G.P., Raschupkin A.V., Zhuravel Y.N. // Computer Optics. – 2015. – Vol. 39(1). – P. 77-82.*

Introduction

Hyperspectral equipment enables to observe emissions in hundreds of very narrow spectral ranges [1]. The multidimensional image, in which two measurements characterize spatial position of ground points and the third one – their spectral properties, is formed in hyperspectral photographing. Each elementary image section called a pixel is followed by a spectral-response characteristic of emission which, when further used in photograph decoding and interpretation, allows to evaluate physicochemical or biological condition of the objects observed.

Remote sensing spacecrafts currently operating and planned for space launching in the coming years (KA EO-1 /USA/, HJ-1B /China/, Resurs-P /Russia/, STSAT-3 /Korea/, ALOS-3 /Japan/, PRISMA /Italy/, EnMAP /Germany/) equipped with hyperspectral equipment don't allow to observe underlying surface with spatial resolution better than 30 m [2].

Current engineering and technological limitations in developing hyperspectral equipment provide a compromise decision on possible achievement of high spectral resolution in exchange for the loss of spatial resolution. Hence, hyperspectral images contain unique data on spectral properties of the objects observed, however the data on their spatial properties contained therein possess less informational content if compared to traditional multispectral photographs.

Therefore, search of technology and research solutions to form, at the same time, images with high spectral and spatial resolution is a critical task to obtain objective information in satellite environmental monitoring.

This paper describes the integration method for hyperspectral and multispectral images to increase their spatial and spectral properties, and it gives proper evaluation data about its efficient performance.

1. RESURS-P Spacecraft

Since July 25th, 2013, the Russian remote sensing spacecraft RESURS-P has been successfully operating in orbit. The important feature of RESURS-P spacecraft that distinguishes it from many other remote sensing spacecrafts is its complex observation capacity due to on-board installation of three types of surveying equipment, i.e. high-detail, wide-span and hyperspectral equipment.

Capability to simultaneously observe underlying surface using different types of surveying equipment significantly improves, among other things, the efficiency of solutions of many social, economic and scientific applied tasks, and creates opportunities to develop new integration methods for the obtained photographs in order to improve their informational properties.

Table 1 shows main characteristics of RESURS-P high-detail multi– and hyperspectral equipment.

Table 1. Main characteristics of RESURS-P equipment

Characteristics	High-detail equipment	Hyperspectral equipment
Ranges of spectral channels, microns	0.45 – 0.52 0.52 – 0.60 0.61 – 0.68 0.67 – 0.70 0.70 – 0.73 0.72 – 0.80 0.80 – 0.90	0.40 – 1.00 (from 96 to 192 channels)
Spatial resolution, m	3	30
Field of view, km	38	30
Image resolution, bits per pixel	10	12

Characteristic properties of RESURS-P surveying equipment enable to simultaneously obtain 7 multispectral photographs within the wave length range from 0.45 to 0.90 microns with spatial resolution of 3 m, and a hypercube of data for the same area with spectral resolution from 5 to 10 nm within the wave length range from 0.4 to 1.00 microns and with spatial resolution of 30 m.

This information enables to define a problem of integration of hyperspectral and multispectral data as follows: to ensure image synthesis possessing both spatial and spectral properties common to specific photographs made by different types of equipment.

2. The offered method

Suppose $X_{MSI} \in P^{M\times N\times k}$ is the multispectral image of underlying surface identified in space P, where M and N are spatial measurements and k means spectral measurements. We similarly define the hyperspectral image

$X_{HSI} \in P^{m\times n\times K}$,

whereas $m << M,\ n << N,\ k << K$.

Suppose that the available images X_{HSI} and X_{MSI} are different versions of the desired image with high spatial and spectral resolution. In this case multi– and hyperspectral images may be conceived as follows:

$X_{MSI} = \Phi_1(X)$,

$X_{HSI} = \Phi_2(X)$,

where $\Phi_1 :\ P^{M\times N\times K} \to P^{M\times N\times k}$

and $\Phi_2 :\ P^{M\times N\times K} \to P^{m\times n\times K}$

are transformation functions of spectral and spatial measurements, respectively.

Taking this into consideration, the integration algorithm of hyperspectral and multispectral images may be presented in the following way in order to increase their informational content.

First, the initial approximation of the desired image $X^{(0)}$ with high spatial and spectral resolution is computed. Each spectral channel of the image $X^{(0)}$ is determined by means of channel interpolation of the multispectral image X_{MSI}:

$$for\ \forall \lambda_q, q = \overline{1,K};$$

$$X^{(0)}(i,j,\lambda_q) = \begin{cases} X_{MSI}(i,j,\lambda_{l-1}) + (X_{MSI}(i,j,\lambda_l) - \\ -X_{MSI}(i,j,\lambda_{l-1}))\cdot\dfrac{\lambda_q-\lambda_{l-1}}{\lambda_l-\lambda_{l-1}}, \\ for\ \lambda_{l-1} \le \lambda_q \le \lambda_l,\ l=\overline{1,k}; \\ X_{MSI}(i,j,\lambda_1) - (X_{MSI}(i,j,\lambda_2) - \\ -X_{MSI}(i,j,\lambda_1))\cdot\dfrac{\lambda_q-\lambda_1}{\lambda_2-\lambda_1}, \\ for\ \lambda_q < \lambda_1; \\ X_{MSI}(i,j,\lambda_k) + (X_{MSI}(i,j,\lambda_k) - \\ -X_{MSI}(i,j,\lambda_{k-1}))\cdot\dfrac{\lambda_q-\lambda_k}{\lambda_k-\lambda_{k-1}}, \\ for\ \lambda_q > \lambda_k \end{cases} \quad (1)$$

$$i=\overline{1,M};\ \ j=\overline{1,N}.$$

Then, the obtained image $X^{(0)}$ is converted to the low resolution hyperspectral image $\tilde{X}_{HSI}$ by reducing spatial dimensionality tenfold using bilinear interpolation.

Approximate estimate of the hyperspectral image $\tilde{X}_{HSI}$ is compared with the original image X_{HSI}, and the following approximation error is computed for each channel:

$$for\ \forall \lambda_q, q = \overline{1,K}$$

$$Error(p,r,\lambda_q) = X_{HSI}(p,r,\lambda_q) - \tilde{X}_{HSI}(p,r,\lambda_q), \quad (2)$$

$$p=\overline{1,m},\ \ r=\overline{1,n}$$

The determined $Error(p,r,\lambda)$ is scaled in accordance with dimensionality of the image $X^{(0)}$ using bilinear interpolation and, finally, initial approximation of the high-resolution hyperspectral image is updated as follows:

$$X(i,j,k) = X^{(0)}(i,j,k) + Error(i,j,k), \quad (3)$$

$$i=\overline{1,M},\ \ j=\overline{1,N},\ \ k=\overline{1,K}.$$

3. Simulated results and evaluation of performance of the hyperspectral and multispectral images integration method

To appraise the offered integration method and to evaluate its performance the aircraft photograph of Baden's suburbs (Switzerland) was used as the test high-resolution hyperspectral image with the dimension of 1500×1000×285 pixels made by APEX [3] equipment. The photograph contains urban in-

frastructure, hydrology, forestry and agricultural facilities registered in 285 spectral channels within the wave length range from 0.413 to 2.421 microns.
Seven images, which are considered to be analogues of RESURS-P multispectral images, were simulated by averaging relevant spectral channels of the original test image. The analogue of RESURS-P multispectral image was formed by selecting first 112 spectral channels within the wave length range from 0.4 to 1.0 micron and by upsampling them with a dimension reduction factor equaled to 10 (Fig.1).

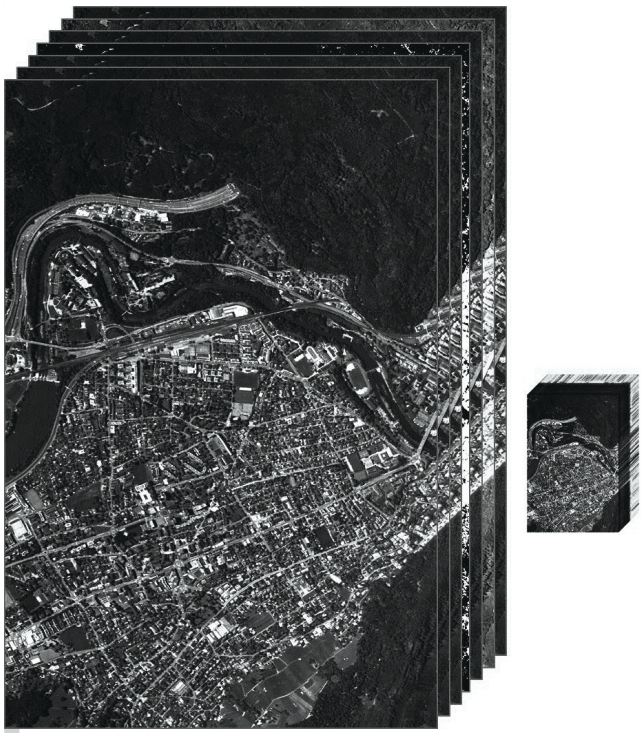

Fig.1 Multi- and hypserspactral images formed

The offered method was simulated on the assumption of that multi– and hyperspectral photographs have undergone procedures of geometrical registration, radiometric and atmospheric correction, and normalization of dynamic light intensity range to the unified quantization scale.
Simulated results are given in Fig.2. Using original and synthesized high-resolution hyperspectral images, the analysis of accuracy of spectral profile reconstruction has been performed. In order to evaluate accuracy of reconstruction of the developed multi– and hyperspectral images integration method, the root-mean-square (RMS) and relative errors characterizing a degree of closeness of original and synthesized images have been used.

$$\varepsilon_{RMS} = \frac{1}{M \cdot N} \sum_{i=1}^{M} \sum_{j=1}^{N} (X(i,j,k) - X^{synthesized}(i,j,k))^2$$

$$\varepsilon_{relative} = \frac{\sum_{i=1}^{M} \sum_{j=1}^{N} (X(i,j,k) - X^{synthesized}(i,j,k))^2}{\sum_{i=1}^{M} \sum_{j=1}^{N} X^2(i,j,k)} \cdot 100\%,$$

where $k = \overline{1,K}$.

Table 2 shows the numerical computation results of evaluation of reconstruction accuracy for each spectral channel of the synthesized high-resolution hyperspectral image.

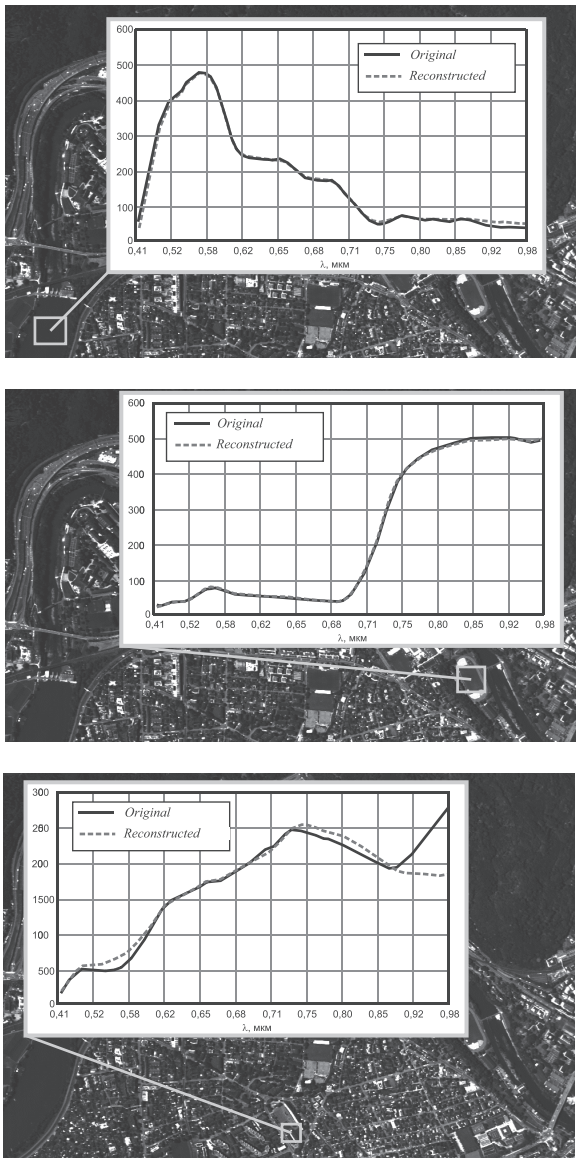

Fig.2 Integration results for multi- and hyperspectral data:
a) water-surface spectral profile reconstruction;
b) foliage spectral profile reconstruction;
c) red roofing spectral profile reconstruction

Table 2. Evaluation results of reconstruction accuracy for each spectral channel

Channel No.	ε_{RMS}	$\varepsilon_{relative},\%$	Channel No.	ε_{RMS}	$\varepsilon_{relative},\%$
1	172.7	57.8	57	123.1	13.1
2	126.0	36.3	58	130.8	13.1
3	93.8	22.6	59	129.2	12.1
4	65.6	13.7	60	118.5	10.2
5	38.6	7.2	61	102.4	8.1
6	16.0	2.7	62	78.2	5.5
7	12.8	2.0	63	46.2	2.9
8	21.0	3.2	64	30.5	1.7
9	28.6	4.3	65	65.5	3.3
10	33.4	5.0	66	106.7	4.9
11	29.9	4.4	67	142.3	6.1
12	24.8	3.6	68	167.5	6.7
13	28.2	3.9	69	180.2	6.8
14	36.9	4.9	70	179.5	6.5
15	44.4	5.7	71	167.0	5.9
16	47.3	6.0	72	148.9	5.1
17	45.3	5.6	73	109.5	3.7
18	40.9	5.0	74	98.1	3.3
19	37.5	4.7	75	100.2	3.3
20	30.7	3.9	76	112.4	3.6
21	24.6	3.1	77	114.2	3.6
22	21.6	2.8	78	112.5	3.5
23	19.1	2.5	79	110.6	3.5
24	18.0	2.3	80	106.6	3.3
25	17.1	2.2	81	99.2	3.1
26	16.7	2.1	82	88.9	2.7
27	16.4	2.1	83	83,5	2.6
28	16.6	2.1	84	75.8	2.3
29	16.4	2.0	85	68.4	2.1
30	15.3	1.9	86	57.4	1.7
31	13.5	1.7	87	47.8	1.4
32	13.0	1.6	88	39.3	1.2
33	13.8	1.7	89	30.5	0.9
34	13.8	1.7	90	25.3	0.8
35	14.0	1.7	91	21.0	0.6
36	14.0	1.7	92	18.3	0.5
37	13.4	1.6	93	23.3	0.7
38	12.0	1.5	94	32.2	1.0
39	10.2	1.2	95	45.7	1.4
40	9.3	1.1	96	63.2	1.9
41	9.4	1.1	97	85.4	2.6
42	10.4	1.2	98	114.3	3.4
43	11.6	1.4	99	147.0	4.4
44	13.1	1.6	100	183.4	5.5
45	16.2	2.0	101	223.0	6.7
46	20.1	2.4	102	266.0	8.0
47	25.0	3.0	103	312.3	9.5
48	30.6	3.7	104	360.7	11.0
49	35.5	4.3	105	410.3	12.5
50	39.9	4.8	106	458.2	14.1
51	43.1	5.2	107	503.7	15.5
52	45.0	5.4	108	545.7	16.7
53	44.9	5.3	109	584.5	17.9
54	39.8	4.7	110	617.1	18.8
55	75.5	8.7	111	642.0	19.4
56	104.5	11.6	112	674.4	20.2
			Mean value:	103.4	5.9

The analysis of Table 2 allows us to conclude that maximum reconstruction errors relate to spectral channels being out of the wave range covered by multispectral photographs. Linear extrapolation used for this purpose gives excessively rough approximation. When cutting off these channels from the data hypercube, reconstruction accuracy of the hyperspectral high-resolution image within the wave range from 0.45 to 0.9 microns will amount to 3.8% that significantly results to high practical use.

The purpose of the next experiment was to determine performance efficiency of the proposed method in tasks of automatic objects' classification. Based on specified spectral data for four types of objects, i.e. water surface, foliage, road surface and blue roofing material, using the Spectrum Angle Mapping (SAM) method [4], a distribution map of these objects was constructed on tested and synthesized hyperspectral images (Fig.3). The visual analysis of the data received confirms high similarity of classification results. To quantify classification results the error matrix was constructed characterizing not only a classification error for each class, but also errors related to false classification. The error matrix of objects' classification based on findings of the conducted experiment is given in Table 3. Matrix rows show true classes of the objects given on a control chart (the initial test hyperspectral image), and matrix columns show the classes outlined on the analyzed map obtained by the synthesized hyperspectral image with high spatial resolution. A sum of diagonal elements of the matrix shows a total number of correctly classified pixels, and the ratio of this amount to the total number of pixels in the matrix is the summary classification accuracy. In Table 3 the correctly classified pixel-wise and percentagewise image areas are bold typed. Summary classification accuracy accounted for 88.5% in all objects. Taking into consideration the fact that this high result was obtained for the synthesized image having essential reconstruction errors in the spectral profile in out-of-range channels covered by multispectral photographs, it can be assumed that the exception of these channels or the use of more accurate extrapolation methods will enable to improve classification quality.

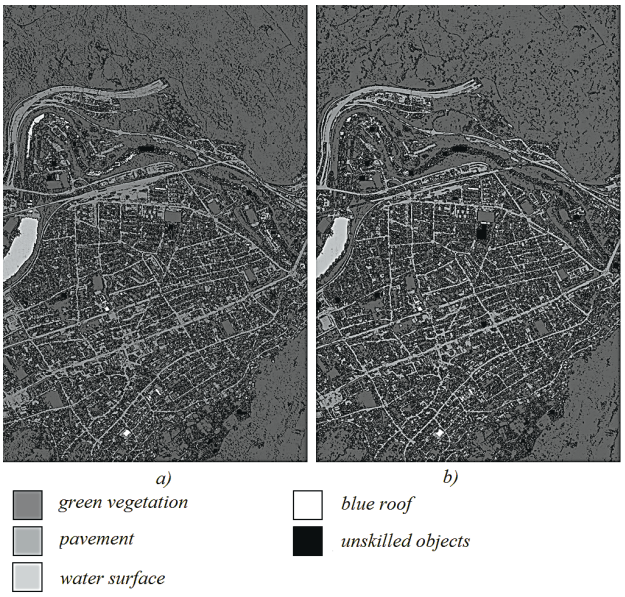

Fig.3 . Results of construction of classification maps: a) initial test image; b) synthesized image

Table 3. Error matrix of channel classification

Class	I	II	III	IV	V
I	**569017** **85.49%**	53107 7.93%	21532 14.12%	302 3.01%	844 40.27%
II	46620 7.00%	**616676** **92.07%**	0 0%	0 0%	0 0%
III	45466 6.83%	0 0%	**131008** **85.88%**	0 0%	0 0%
IV	4263 0.64%	0 0%	0 0%	**9722** **96.99%**	0 0%
V	191 0.03%	0 0%	0 0%	0	**1252** **59.73%**
Σ	665557 100%	669783 100%	152540 100%	10024 100%	2096 100%

The following class designations are given in Table 3: I – unclassified objects, II – foliage, III – road surface, IV – water surface, V – blue roofing.

Conclusion

The offered hyperspectral and multispectral data integration method is simple enough both intuitively and computationally. The method allows us to synthesize images which combine spatial and spectral properties common for particular multi– and hyperspectral photographs. Testing and experimental studies of the method performance have demonstrated its potential opportunities and high accuracy in tasks of objects' classification. The subject of further researches is to search proper solutions on how to improve reconstruc-

tion accuracy of signals being out of wave range covered with multispectral photographs.

The offered method may be used to create a new information product required to solve social, economic and scientific applied tasks which demand from space surveying both high spatial and spectral resolution.

Acknowledgements

The work has been performed with financial support from RFBR (the Russian Foundation for Basic Researches) grant "OFI_M" No. 13-01-12014.

References

1. Shaw, G.A. Spectral Imaging for Remote Sensing /G.A. Shaw, H.K. Burke // Lincoln Laboratory Journal. – 2003. –Vol. 14(1). – P. 3-28.

2. https://eoportal.org/web/eoportal/satellite-missions.

3. http://www.apex-esa.org/content/free-data-cubes.

4. Rashmi, S. Spectral Angle Mapper Algorithm for Remote Sensing Image Classification / S. Rashmi, S. Addamani, Venkat, S. Ravikiran // IJISET – International Journal of Innovative Science, Engineering & Technology. – 2014. – Vol. 1(4). – P. 201-205.